

Supporting Information

Ru_xCr_{1-x}O_y Fiber-in-Tube as Highly Efficient Electrocatalysts for pH-Universal Water Oxidation *via* Facile Bubble Desorption

Chaewon Song,¹ Dasol Jin,¹ Subin Choi, Youngmi Lee*

Department of Chemistry & Nanoscience, Ewha Womans University, Seoul 03760, Republic of Korea

¹Equally contributed to this work

*Corresponding author: youngmilee@ewha.ac.kr (Y. L.)

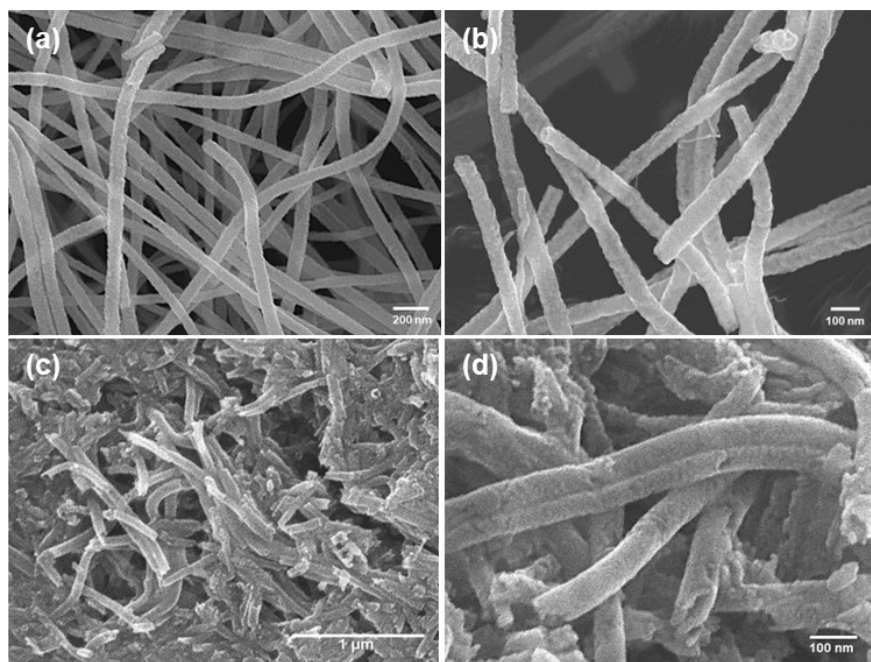


Fig. S1. SEM images of synthesized (a,b) Ru/RuO₂ and (c,d) Cr₂O₃.

Table S1. EDS analysis results for the $\text{Ru}_x\text{Cr}_{1-x}\text{O}_y_n$ NFs (mean \pm standard deviation), which were analyzed at more than 20 places.

Catalyst	Atomic %	
	Ru	Cr
$\text{Ru}_x\text{Cr}_{1-x}\text{O}_y_5$	45.98 (\pm 1.08)	54.02 (\pm 1.08)
$\text{Ru}_x\text{Cr}_{1-x}\text{O}_y_20$	47.00 (\pm 1.04)	53.00 (\pm 1.04)
$\text{Ru}_x\text{Cr}_{1-x}\text{O}_y_50$	45.74 (\pm 0.69)	54.26 (\pm 0.69)
$\text{Ru}_x\text{Cr}_{1-x}\text{O}_y_100$	46.50 (\pm 0.68)	53.50 (\pm 0.68)

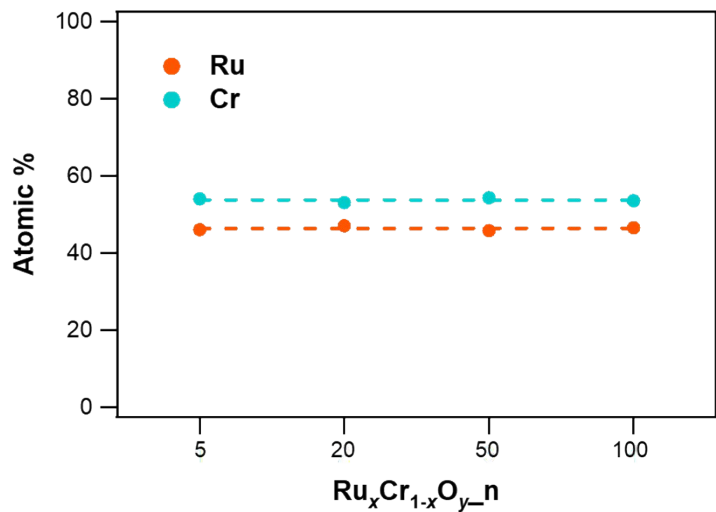


Fig. S2. The relative atomic composition ratios (Ru/Cr) for the $\text{Ru}_x\text{Cr}_{1-x}\text{O}_y\text{-n}$, which were analyzed at more than 20 places through EDS.

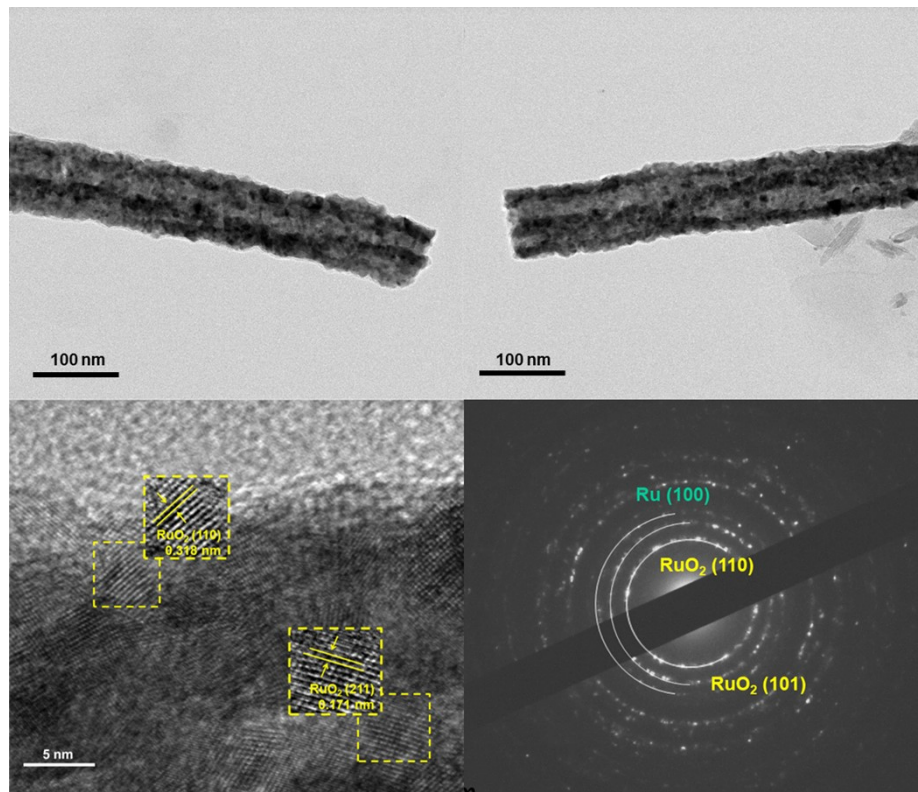


Fig. S3. (a,b) Low-magnification TEM images, (c) HRTEM image and (d) SAED pattern of Ru/RuO₂.

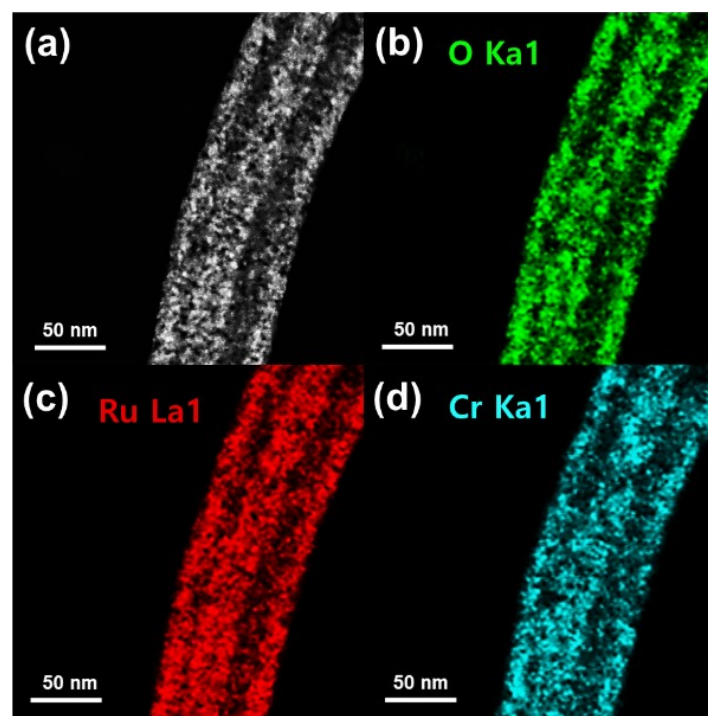


Fig. S4. TEM analysis results of $\text{Ru}_x\text{Cr}_{1-x}\text{O}_y\text{-}20$: (a) Low-magnification TEM image and (b-d) elemental mapping analysis of O (green), Ru (red), Cr (cyan).

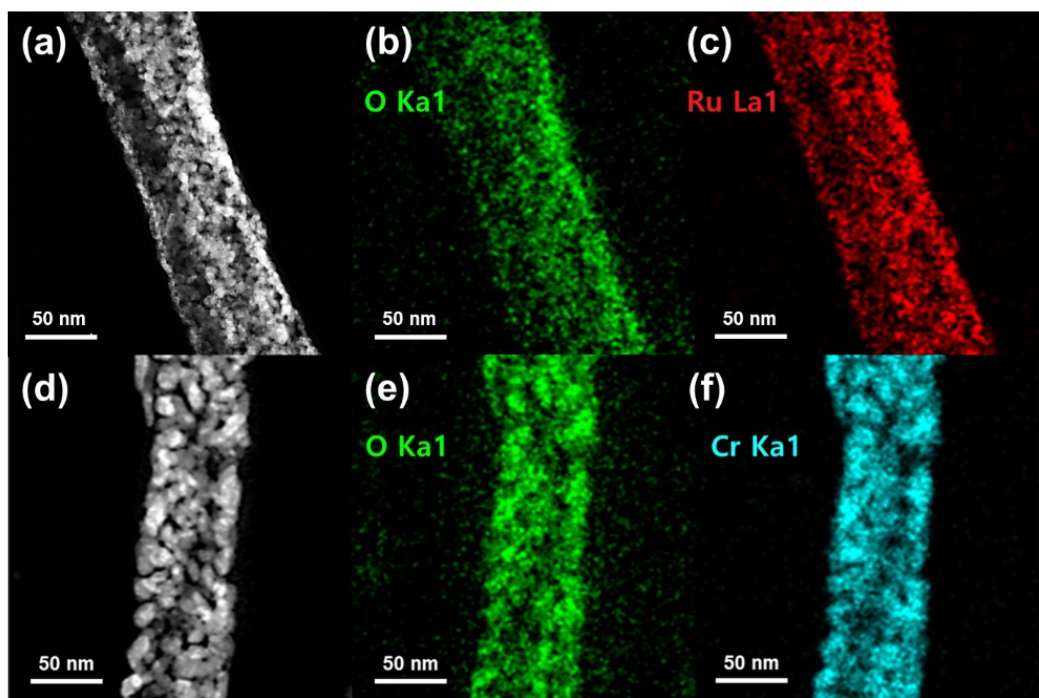


Fig. S5. TEM analysis results of (a-c) Ru/RuO₂ (d-f) Cr₂O₃: (a,d) Low-magnification TEM images and (b,c,e,f) elemental mapping analysis of O (green), Ru (red), Cr (cyan).

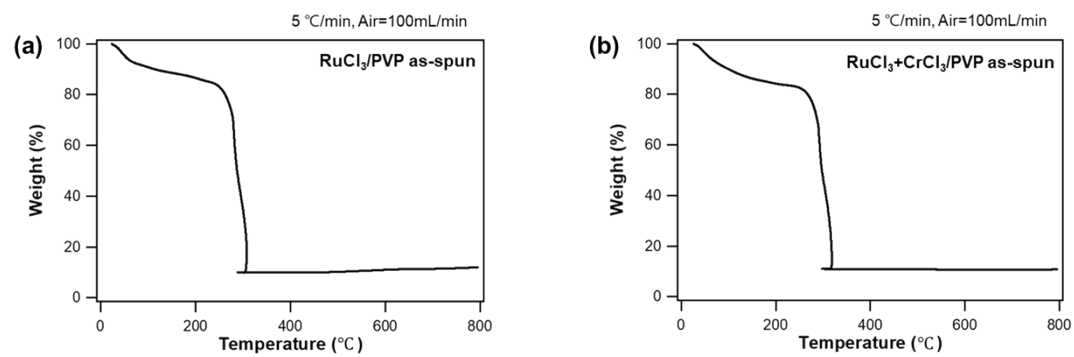


Fig. S6. Thermogravimetric analysis (TGA) curves of (a) RuCl₃/PVP as-spun and (b) RuCl₃+CrCl₃/PVP as-spun.

Table S2. Full width at half maximum (FWHM) and **crystallite sizes of**
Ru_xCr_{1-x}O_y_n.

Catalyst	Ru _x Cr _{1-x} O _y _5	Ru _x Cr _{1-x} O _y _20	Ru _x Cr _{1-x} O _y _50	Ru _x Cr _{1-x} O _y _100
FWHM (2θ)	1.60	1.34	0.407	0.382
Crystallite size (nm)	5.34	6.38	21.00	22.38

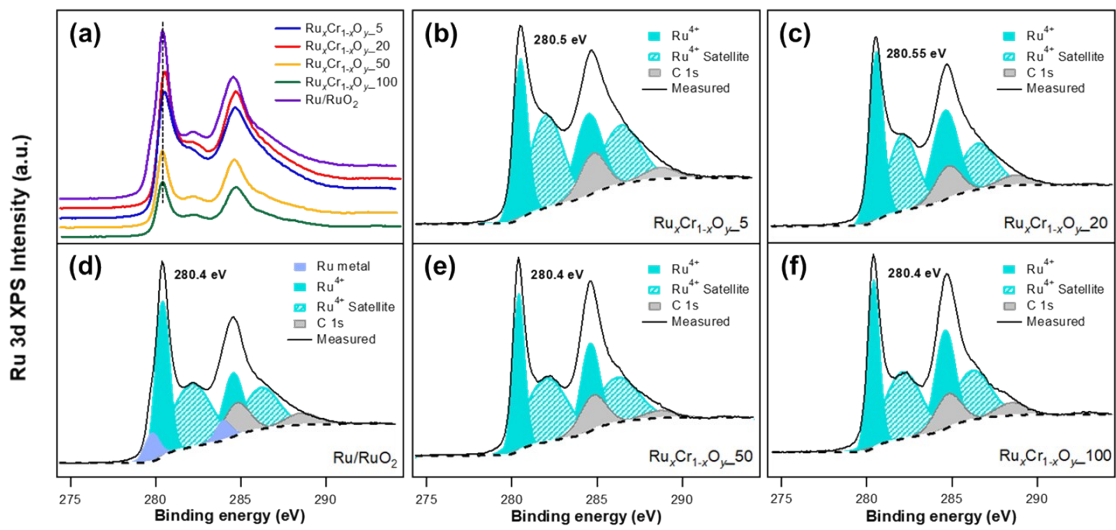


Fig. S7. XPS spectra of the synthesized nanomaterials: $\text{Ru}_x\text{Cr}_{1-x}\text{O}_y$ -*n* NFs (*n* = 5, 20, 50, 100) and Ru/RuO_2 for Ru 3d.

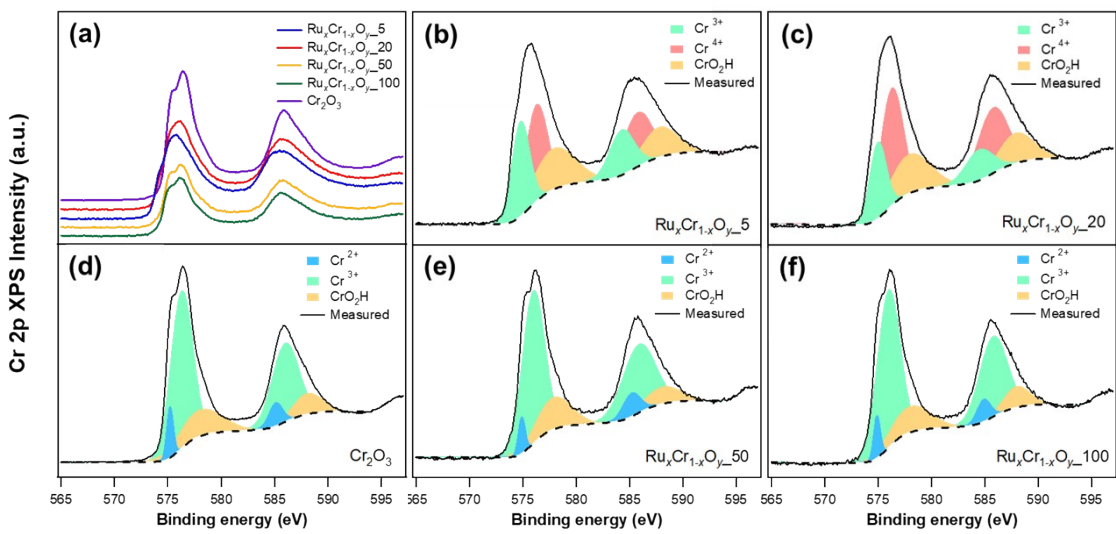


Fig. S8. XPS spectra of the synthesized nanomaterials: $\text{Ru}_x\text{Cr}_{1-x}\text{O}_y$ ($n = 5, 20, 50, 100$) and Cr_2O_3 for Cr 2p.

Table S3. Elemental profiling of $\text{Ru}_x\text{Cr}_{1-x}\text{O}_y_20$ using XPS etching technique. Note that the unit for the elemental distribution is in atomic percent (%).

Catalyst	Non etching (Surface)			15 s etching			30 s etching		
	Ru	Cr	O	Ru	Cr	O	Ru	Cr	O
$\text{Ru}_x\text{Cr}_{1-x}\text{O}_y_20$	13.55	14.35	72.10	15.63	16.02	68.35	16.81	16.66	66.53

Table S4. Comparison of the mass activities of the samples at 1.49 V (vs. RHE) in 1 M KOH, 0.5 M PBS (pH 7.2) and 0.5 M H₂SO₄ solutions.

Solution	Sample	Mass activity (A cm ⁻² mg _{Ru or Ir} ⁻¹)
1 M KOH	Ru _x Cr _{1-x} O _y _20	0.1
	Ir/C	0.1
0.5 M PBS (pH 7.2)	Ru _x Cr _{1-x} O _y _20	0.04
	Ir/C	0.01
0.5 M H ₂ SO ₄	Ru _x Cr _{1-x} O _y _20	0.3
	Ir/C	0.2

Table S5. Comparison of Tafel slopes and potentials of $\text{Ru}_x\text{Cr}_{1-x}\text{O}_y_n$ at current density of 10 mA cm⁻² for the synthesized nanomaterials and Ir/C in pH-universal aqueous solutions.

Electrolyte	Catalyst	Potential@10 mA cm ⁻² (V vs. RHE)	Tafel slope (mV dec ⁻¹)
1 M KOH	$\text{Ru}_x\text{Cr}_{1-x}\text{O}_y_5$	1.48	40.4
	$\text{Ru}_x\text{Cr}_{1-x}\text{O}_y_20$	1.47	37.5
	$\text{Ru}_x\text{Cr}_{1-x}\text{O}_y_50$	1.56	74.0
	$\text{Ru}_x\text{Cr}_{1-x}\text{O}_y_100$	1.59	85.9
	RuO_2/Ru	1.51	99.7
	Cr_2O_3	2.46	322.6
	Ir/C	1.53	52.7
0.5 M PBS (pH 7.2)	$\text{Ru}_x\text{Cr}_{1-x}\text{O}_y_5$	1.49	75.7
	$\text{Ru}_x\text{Cr}_{1-x}\text{O}_y_20$	1.49	68.9
	$\text{Ru}_x\text{Cr}_{1-x}\text{O}_y_50$	1.58	112.1
	$\text{Ru}_x\text{Cr}_{1-x}\text{O}_y_100$	1.63	140.5
	RuO_2/Ru	1.58	115.8
	Cr_2O_3	2.61	343.3
	Ir/C	1.73	306.7
0.5 M H₂SO₄	$\text{Ru}_x\text{Cr}_{1-x}\text{O}_y_5$	1.44	43.1
	$\text{Ru}_x\text{Cr}_{1-x}\text{O}_y_20$	1.44	40.8
	$\text{Ru}_x\text{Cr}_{1-x}\text{O}_y_50$	1.48	58.6
	$\text{Ru}_x\text{Cr}_{1-x}\text{O}_y_100$	1.48	76.2
	RuO_2/Ru	1.48	48.8
	Cr_2O_3	2.34	273.2
	Ir/C	1.52	67.1

Table S6. Comparison of the Tafel slope and overpotential corresponding to 10 mA cm⁻² for Ru_xCr_{1-x}O_y _20 and other previously reported Ru-based electrocatalysts in alkaline media.

Catalyst	Electrolyte	Overpotential (mV) @10mA cm ⁻²	Tafel slope (mV dec ⁻¹)	Reference
Ru _x Cr _{1-x} O _y _20	1 M KOH	240	37.5	This work
^a Co-Ru-Py@500	1 M KOH	230	50	[67]
^b Ru/Co-N-C-800°C	1 M KOH	276	55.7	[56]
^c RuNi ₁ Co ₁ @CMT	1 M KOH	299	83	[68]
^d D-RuO ₂ /TiO ₂ /TM	1 M KOH	296	46.6	[69]
^e HP-RuO ₂	1 M KOH	242	62	[57]
^f RuCu NSs	1 M KOH	234	43	[70]
^g RuIrO _x	1 M KOH	250	50	[18]
^h Ru-H ₂ O/CC-350	1 M KOH	266	73.45	[71]
ⁱ Ru/NF-2	1 M KOH	330	62	[72]

^aCo-Ru-Py@500 represents RuO₂-CoO_x nanoparticles with an ultra-thin coated carbon layer. ^bRu/Co-N-C-800°C represents atomically dispersed Ru/Co on the nitrogen–carbon support. ^cRuNi₁Co₁@CMT represents ruthenium-nickel-cobalt alloy nanoparticles embedded in the hollow carbon tubes. ^dD-RuO₂/TiO₂/TM represents a defective RuO₂/TiO₂ nano-heterostructure catalyst on Ti mesh. ^eHP-RuO₂ represents the hierarchical porous nanostructures riveted with ultrafine Ru nanoclusters. ^fRuCu NSs represents channel rich RuCu nanosheets. ^gRuIrO_x represents RuIrO_x (x ≥ 0) nano-net cage catalyst. ^hRu-H₂O/CC-350 represents Ru nanoparticles on carbon cloth. ⁱRu/NF-2 represents Ru-loaded Ni foam.

Table S7. Comparison of the Tafel slope and overpotential corresponding to 10 mA cm⁻² for Ru_xCr_{1-x}O_y _20 and other previously reported Ru-based electrocatalysts in neutral media.

Catalyst	Electrolyte	Overpotential (mV) @10mA cm ⁻²	Tafel slope (mV dec ⁻¹)	Reference
Ru _x Cr _{1-x} O _y _20	0.5 M PBS	260	68.9	This work
^a Ru@Co-B/NF	0.5 M PBS	257	105.3	[61]
^b HP-RuO ₂	1.0 M PBS	262	93	[57]
^c a/c-RuO ₂	1 M PBS	287	82.9	[16]
^d Ni/RuO _x @C	1 M PBS	316	89	[59]
^e Ru _{0.5} Ir _{0.5}	1.0 M PBS	248	127	[62]
^f RuO ₂ /Co ₃ O ₄	1 M PBS	365	53	[63]
^g SCN-Ru-RuO ₂ /C ₃ N ₄ -2	1 M PBS (pH=7.0)	342	92	[64]
^h RuCo@CDs	1.0 M PBS	410	147.4	[65]
ⁱ Ru-RuO ₂ /CNT	1.0 M PBS	275	97	[66]

^aRu@Co-B/NF represents ruthenium modified cobalt boride on Ni foil. ^bHP-RuO₂ represents the hierarchical porous nanostructures riveted with ultrafine Ru nanoclusters. ^ca/c-RuO₂ represents amorphous/crystalline heterophase rutile-structured RuO₂. ^dNi/RuO_x@C represents Ru/RuO_x/NiO nanoparticles into N-doped carbon matrix. ^eRu_{0.5}Ir_{0.5} represents unsupported Ru_{0.5}Ir_{0.5} alloy. ^fRuO₂/Co₃O₄ represents RuO₂-decorated Co₃O₄ nanorod arrays. ^gSCN-Ru-RuO₂/C₃N₄-2 represents the thiocyanate modified Ru-RuO₂/C₃N₄. ^hRuCo@CDs represents Ru with Co-doped carbon dots. ⁱRu-RuO₂/CNT represents Ru-RuO₂ hybrid nanoparticles decorating carbon nanotube composites.

Table S8. Comparison of the Tafel slope and overpotential corresponding to 10 mA cm⁻² for Ru_xCr_{1-x}O_y _20 and other previously reported Ru-based electrocatalysts in acidic media.

Catalyst	Electrolyte	Overpotential (mV) @10mA cm ⁻²	Tafel slope (mV dec ⁻¹)	Reference
Ru _x Cr _{1-x} O _y _20	0.5 M H ₂ SO ₄	210	40.8	This work
^a Cr _{0.6} Ru _{0.4} O ₂ (550)	0.5 M H ₂ SO ₄	178	58	[43]
^b Cu-RuO ₂ -300	0.5 M H ₂ SO ₄	201	55	[54]
^c SS Pt-RuO ₂ HNSs	0.5 M H ₂ SO ₄	228	51.0	[55]
^d Ru/Co-N-C-800 °C	0.5 M H ₂ SO ₄	232	67.5	[56]
^e HP-RuO ₂	0.5 M H ₂ SO ₄	209	72	[57]
^f Ru ₃ Ni ₃ NAs	0.5 M H ₂ SO ₄	252	45.8	[58]
^g Ni/RuO _x @C	0.5 M H ₂ SO ₄	211	46	[59]
^h RuIrTe NTs	0.5 M H ₂ SO ₄	205	41.2	[60]
ⁱ RuIrO _x	0.5 M H ₂ SO ₄	233	42	[18]
^j RuOCl@MnO _x	0.5 M H ₂ SO ₄	228	43	[73]

^aCr_{0.6}Ru_{0.4}O₂ (550) represents rutile structured chromium-ruthenium oxide. ^bCu-RuO₂-300 represents Cu-doped RuO₂. ^cSS Pt-RuO₂ HNSs represents single-site Pt-doped RuO₂ hollow nanospheres. ^dRu/Co-N-C-800 °C represents atomically dispersed Ru/Co on the nitrogen–carbon support. ^eHP-RuO₂ represents the hierarchical porous nanostructures riveted with ultrafine Ru nanoclusters. ^fRu₃Ni₃ NAs represents Ru-Ni nanosheet assemblies. ^gNi/RuO_x@C represents peroxidized NiRu alloy nanoparticles into N-doped carbon matrix. ^hRuIrTe NTs represents RuIrTe nanotubes. ⁱRuIrO_x represents RuIrO_x (x ≥ 0) nano-netcage catalyst.

Table S9. Comparison of properties of previously reported OER catalysts.

Reference	Specific catalyst structure	Synthesis method	OER performance		Stability
			Tafel Slope	Overpotential at 10 mA cm ⁻²	
This study	Fiber-in-tube shaped Ru _x Cr _{1-x} O _y _20	(1) Electrospinning (2) O ₂ -Calcination	(1) Alkaline : 37.5 mV dec ⁻¹ (2) Neutral : 68.9 mV dec ⁻¹ (3) Acidic : 40.8 mV dec ⁻¹	(1) Alkaline : 240 mV (vs. RHE) (2) Neutral : 260 mV (vs. RHE) (3) Acidic : 210 mV (vs. RHE)	Spontaneous OER performance using chronopotentiometric technique for 20 hours under pH-universal conditions. Following the extended OER operation, physicochemical analysis of the catalysts was carried out to verify their structural stability.
[74]	Nanoneedle structure of P-Ce SAs@CoO	(1) Ar plasma process (2) Ce-ion electrodeposition (3) Vacancy-assisted anchoring method	75 mV dec ⁻¹ in alkaline condition	261 mV	Chronoamperometric current-time (<i>i</i> -t) test for 27 hours, and basic structural unit and composition of the catalyst after stability test were verified.
[75]	Nanoneedle arrays for Ce-CoP@CC	(1) Thermal reaction using Teflon-lined steel reactor (2) Phosphorization	50.39 mV dec ⁻¹ in alkaline condition	240 mV	Chronoamperometric current-time (<i>i</i> -t) test for 27 hours, and basic structural and surface chemical state of the catalyst after stability test were verified.

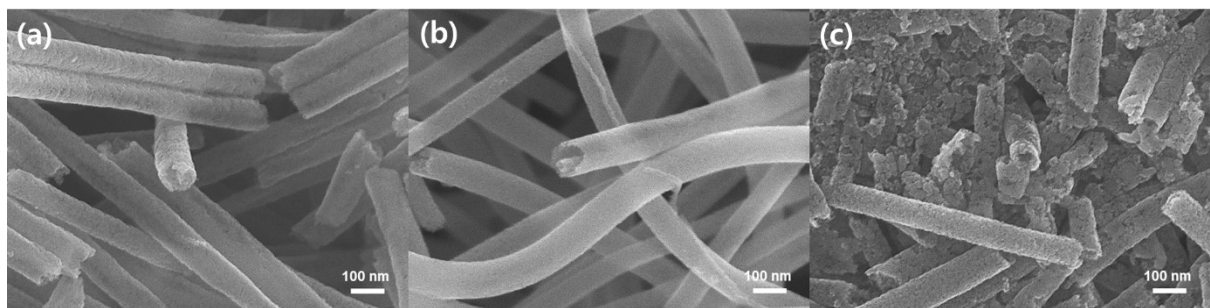


Fig. S9. SEM images of (a) $\text{Ru}_{0.73}\text{Cr}_{0.27}\text{O}_y$, (b) $\text{Ru}_{0.47}\text{Cr}_{0.53}\text{O}_y$ and (c) $\text{Ru}_{0.27}\text{Cr}_{0.73}\text{O}_y$, respectively. Note that $\text{Ru}_x\text{Cr}_{1-x}\text{O}_y_20$ was represented as $\text{Ru}_{0.47}\text{Cr}_{0.53}\text{O}_y$ with chemical formulas corresponding to their molar ratios for the purpose of comparison.

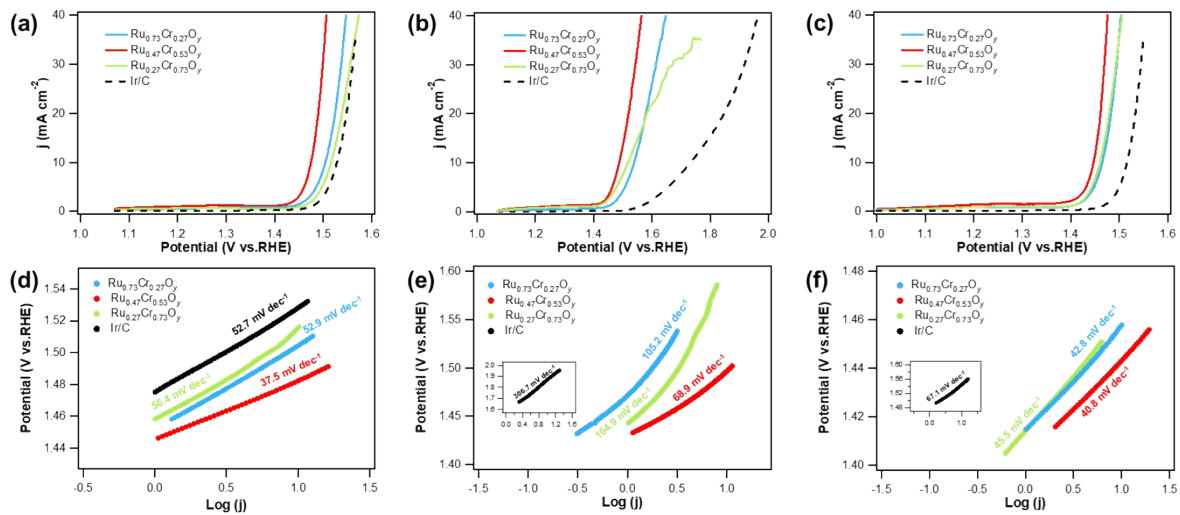


Fig. S10. Comparison of OER performances in Ar-saturated aqueous solution of (a,d) 1.0 M KOH, (b,e) 0.5 M PBS (pH 7.2) and (c,f) 0.5 M H₂SO₄: (a-c) RDE polarization curves with *iR* compensation obtained using GC electrodes modified with Ru_xCr_{1-x}O_y ($x = 0.27, 0.47$ and 0.73) at a scan rate of 10 mV s^{-1} and a rotating speed of 1600 rpm. (d-f) The corresponding Tafel plots for the OER obtained from RDE curves recorded at 1 mV s^{-1} .

Table S10. Comparison of the OER activities of the synthesized nanomaterials composed of various Ru/Cr ratios in 1.0 M KOH, 0.5 M PBS (pH 7.2) and 0.5 M

Electrolyte	Catalyst	Potential@10 mA cm ⁻² (V vs. RHE)	Tafel slope (mV dec ⁻¹)
1.0 M KOH	Ru _{0.73} Cr _{0.27} O _y	1.50	52.9
	Ru _{0.43} Cr _{0.57} O _y	1.47	37.5
	Ru _{0.27} Cr _{0.73} O _y	1.52	56.4
0.5 M PBS (pH 7.2)	Ru _{0.73} Cr _{0.27} O _y	1.54	105.2
	Ru _{0.43} Cr _{0.57} O _y	1.49	68.9
	Ru _{0.27} Cr _{0.73} O _y	1.52	164.9
0.5 M H ₂ SO ₄	Ru _{0.73} Cr _{0.27} O _y	1.46	42.8
	Ru _{0.43} Cr _{0.57} O _y	1.44	40.8
	Ru _{0.27} Cr _{0.73} O _y	1.46	45.5

H₂SO₄ media.

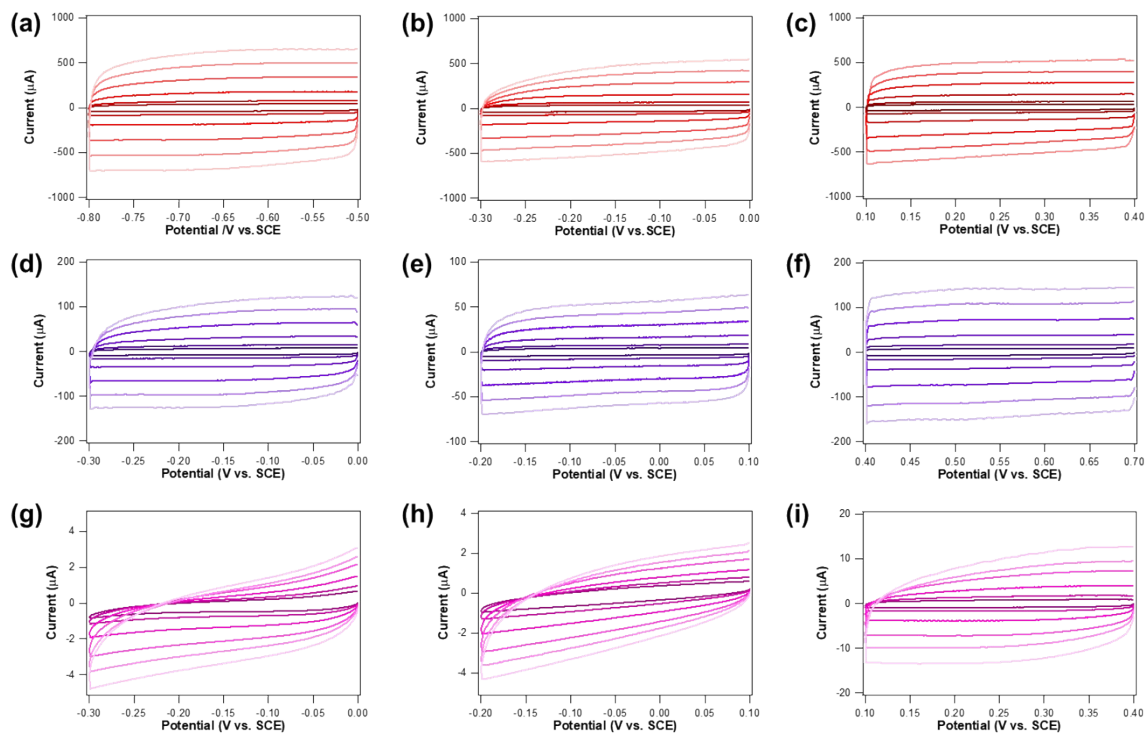


Fig. S11. Cyclic voltammograms of (a-c) $\text{Ru}_x\text{Cr}_{1-x}\text{O}_y\text{-}20$, (d-e) Ru/RuO_2 and (g-i) Cr_2O_3 in (a,d,g) 1 M KOH, (b,e,h) 0.5 M PBS (pH 7.2) and (c,f,i) 0.5 M H_2SO_4 at various scan rates of 10, 20, 50, 100, 150 and 200 mV s^{-1} .

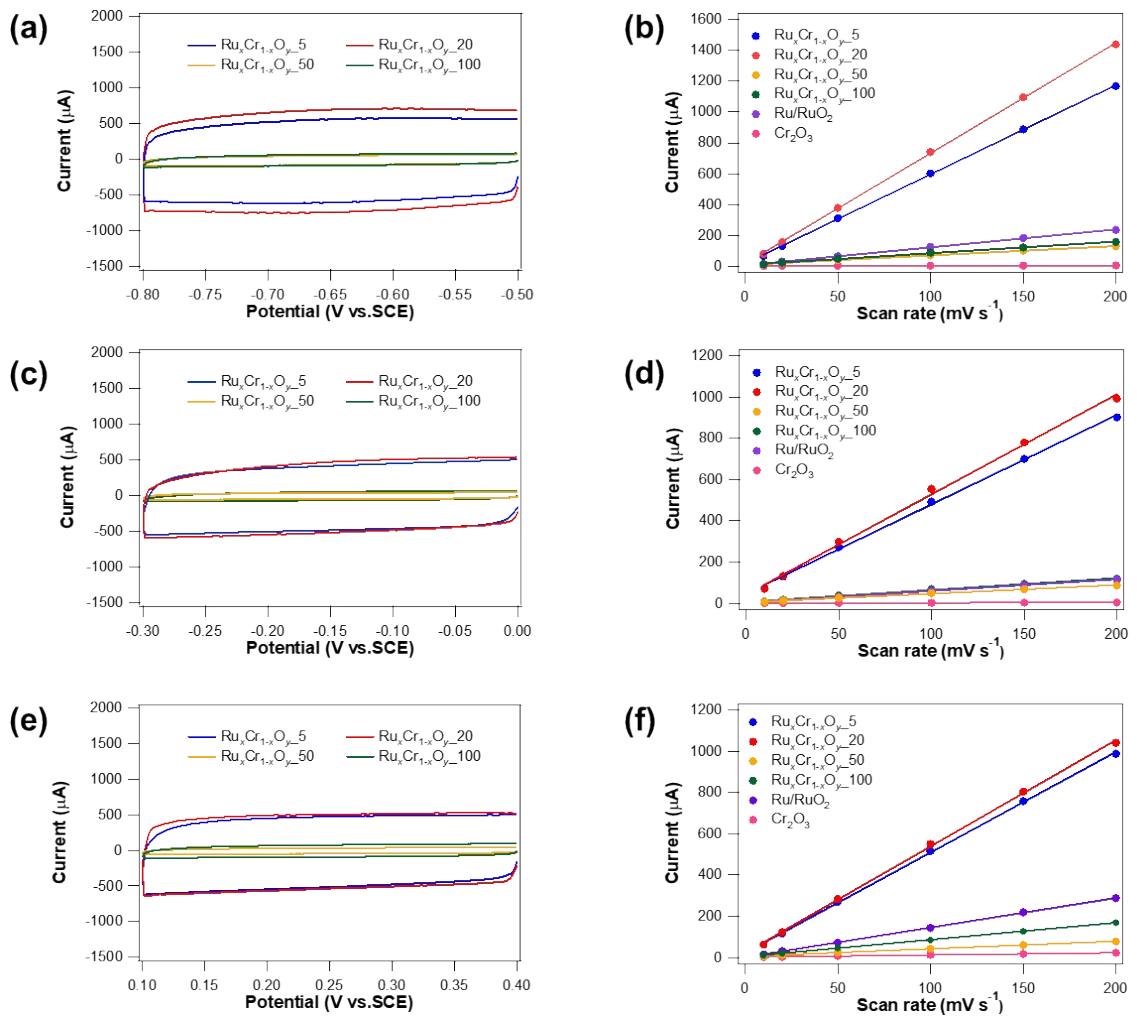


Fig. S12. Cyclic voltammograms of $\text{Ru}_x\text{Cr}_{1-x}\text{O}_y-n$ measured in (a) 1 M KOH, (b) 0.5 M PBS (pH 7.2) and (c) 0.5 M H_2SO_4 solutions at a scan rate of 200 mV s^{-1} . The plots of cathodic-anodic current difference (Δi) versus various scan rate (10, 20, 50, 100, 150, 200 mV s^{-1}) were obtained in (d) 1 M KOH, (e) 0.5 M PBS (pH 7.2) and (f) 0.5 M H_2SO_4 .

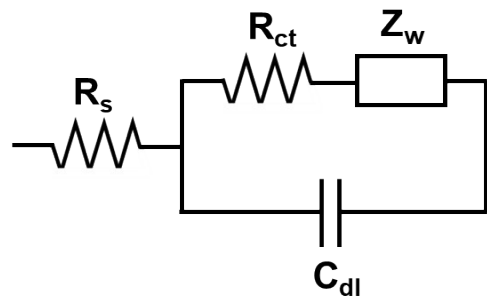


Fig. S13. Equivalent circuit diagram for EIS analysis.

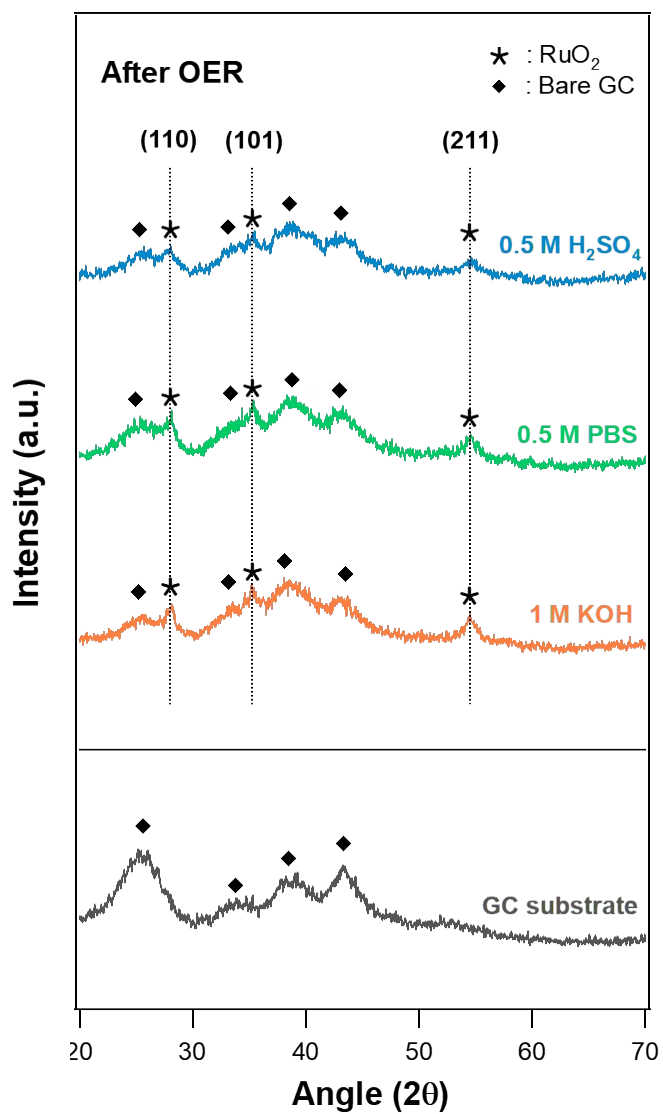


Fig. S14. XRD patterns of Ru_xCr_{1-x}O_y_20 after stability test for 20 h under universal pH conditions (i.e., 1 M KOH, 0.5 M PBS (pH 7.2) and 0.5 M H₂SO₄).

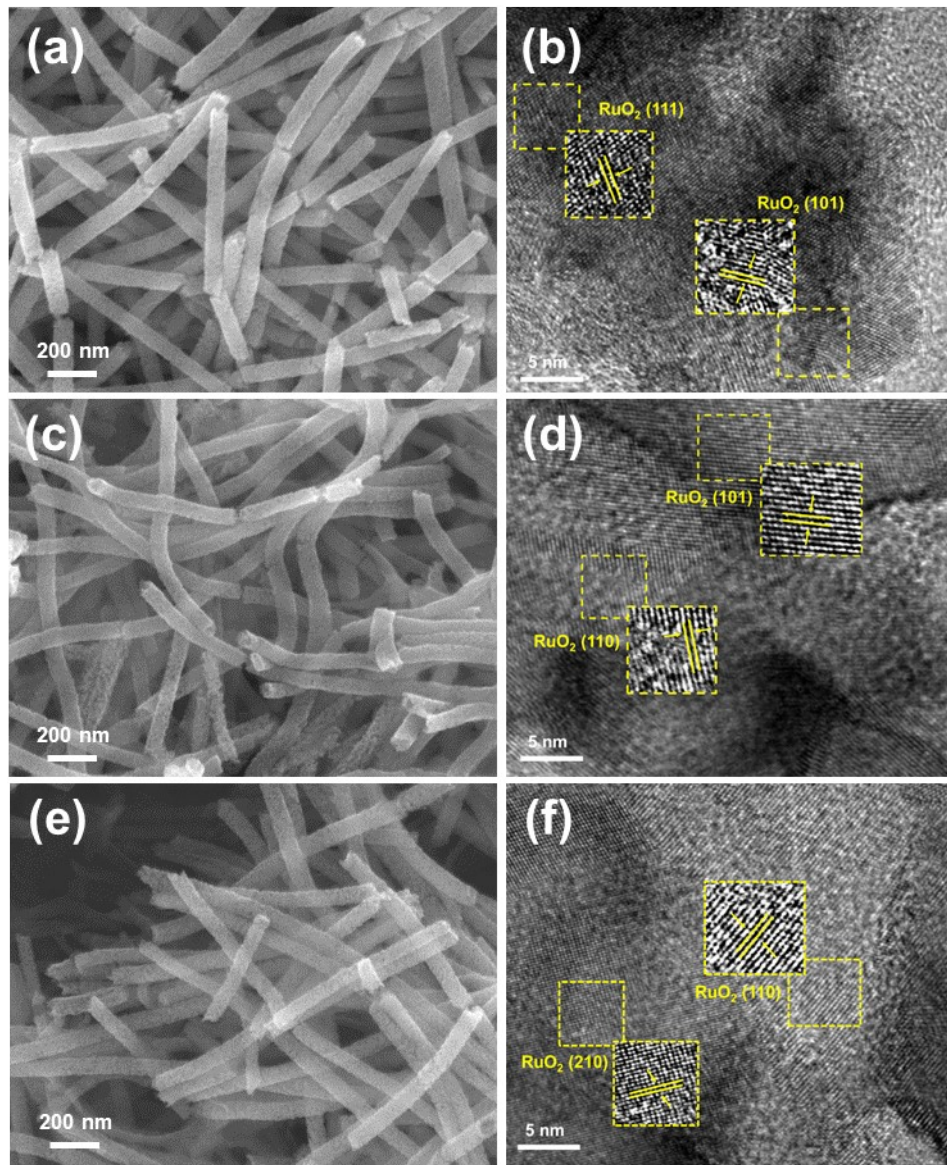


Fig. S15. (a) SEM image, (b) Low-magnification TEM image, (c) HRTEM image and (d) SAED pattern of $\text{Ru}_x\text{Cr}_{1-x}\text{O}_y\text{-20}$ after stability test in 1 M KOH aqueous solution for 20 h.

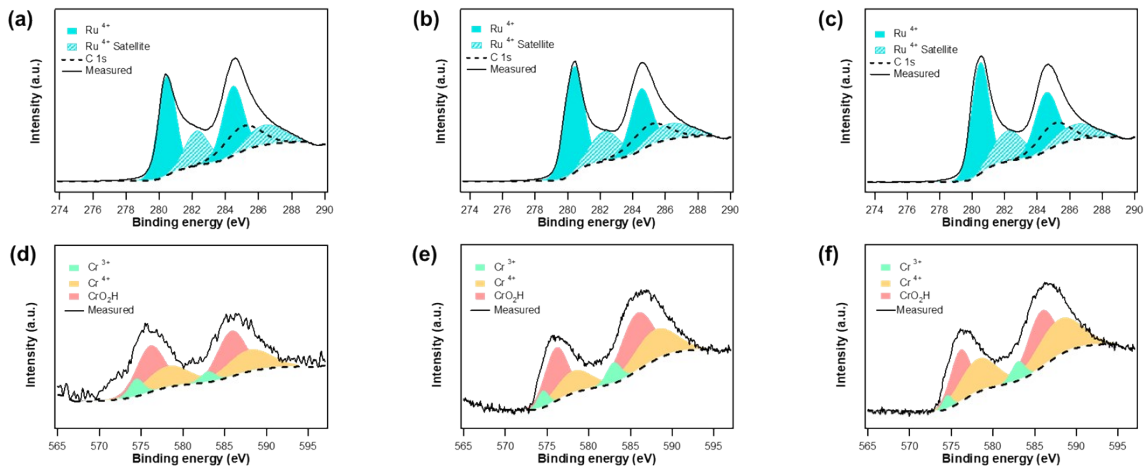


Fig. S16. High resolution XPS spectra of (a-c) Ru 3d and (d-f) Cr 2p regions for $\text{Ru}_x\text{Cr}_{1-x}\text{O}_y_20$ after stability test for 20 h in (a,d) 1 M KOH, (b,e) 0.5 M PBS (pH 7.2) and (c,f) 0.5 M H_2SO_4 solutions, respectively.

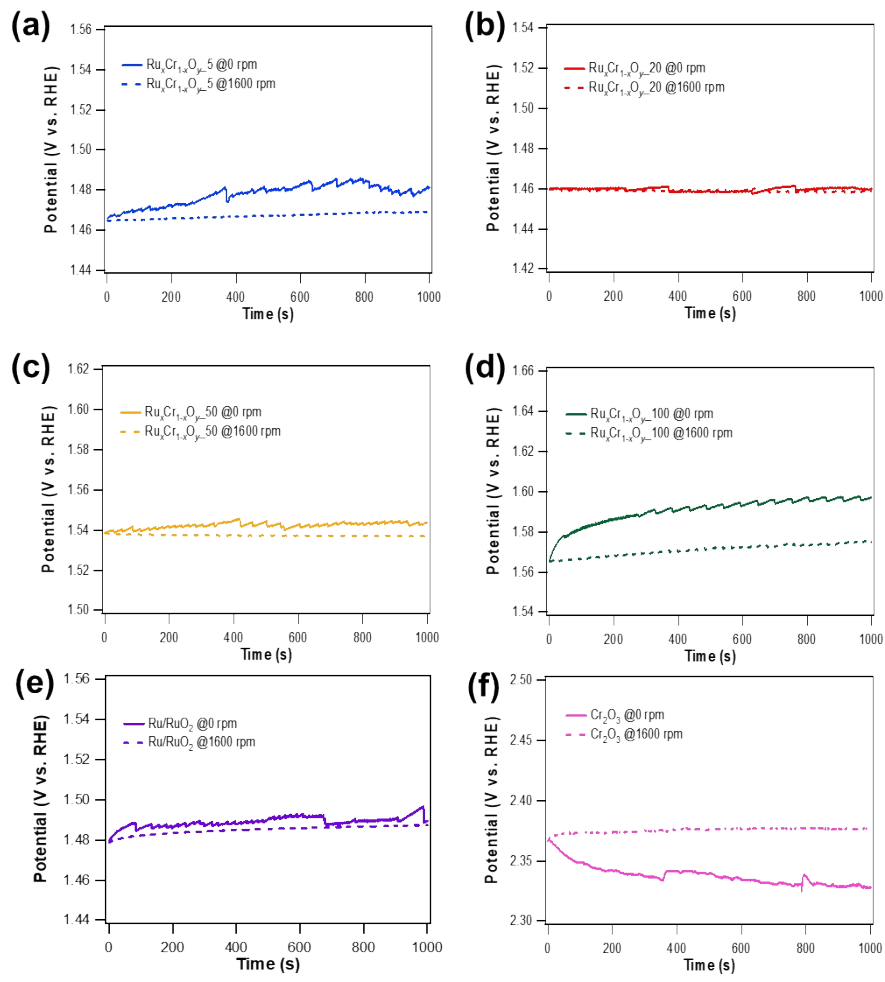


Fig. S17. Chronopotentiometric monitoring of generated O_2 gas desorption for (a) $\text{Ru}_{x}\text{Cr}_{1-x}\text{O}_{y-5}$, (b) $\text{Ru}_{x}\text{Cr}_{1-x}\text{O}_{y-20}$, (c) $\text{Ru}_{x}\text{Cr}_{1-x}\text{O}_{y-50}$, (d) $\text{Ru}_{x}\text{Cr}_{1-x}\text{O}_{y-100}$, (e) RuO_2/Ru and (f) Cr_2O_3 in 1 M KOH aqueous solution. Constant current of 5 mA cm^{-2} was applied for 1000-s continuous OER.

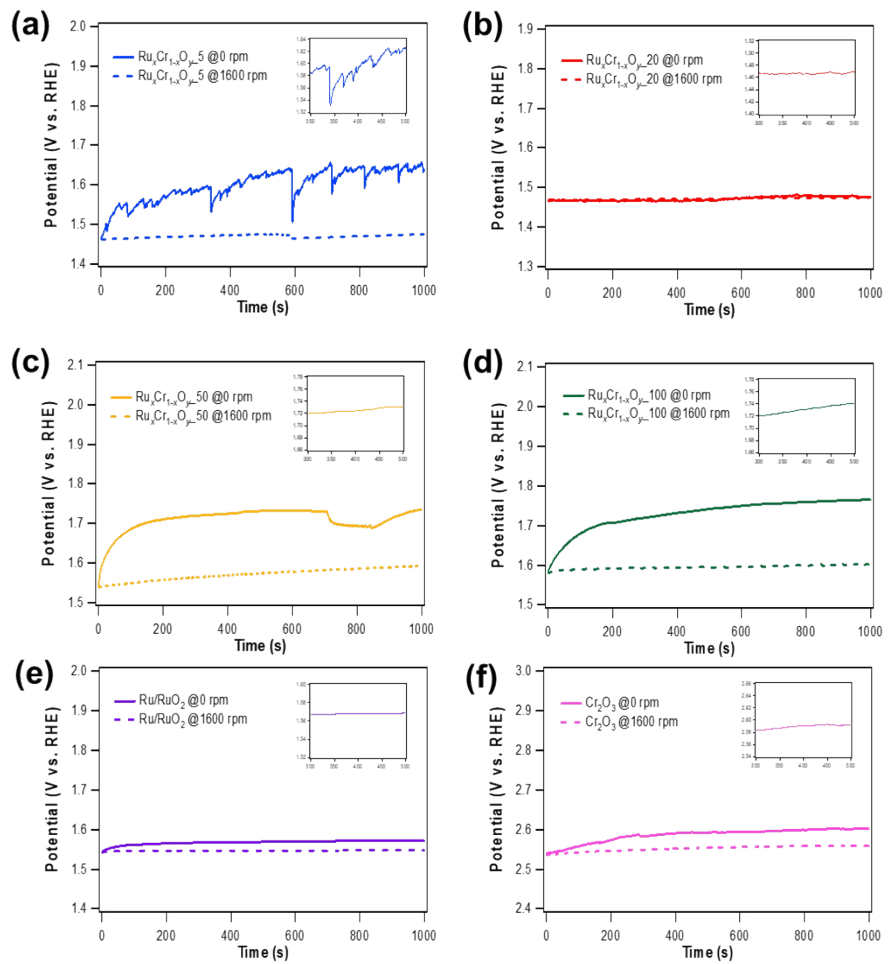


Fig. S18. Chronopotentiometric monitoring of generated O_2 gas desorption for (a) $Ru_xCr_{1-x}O_y_5$, (b) $Ru_xCr_{1-x}O_y_20$, (c) $Ru_xCr_{1-x}O_y_50$, (d) $Ru_xCr_{1-x}O_y_100$, (e) Ru/RuO_2 and (f) Cr_2O_3 in 0.5 M PBS (pH 7.2) aqueous solution. Constant current of 5 mA cm^{-2} was applied for 1000-s continuous OER (Insets: potential changes measured between 300 and 500 s).

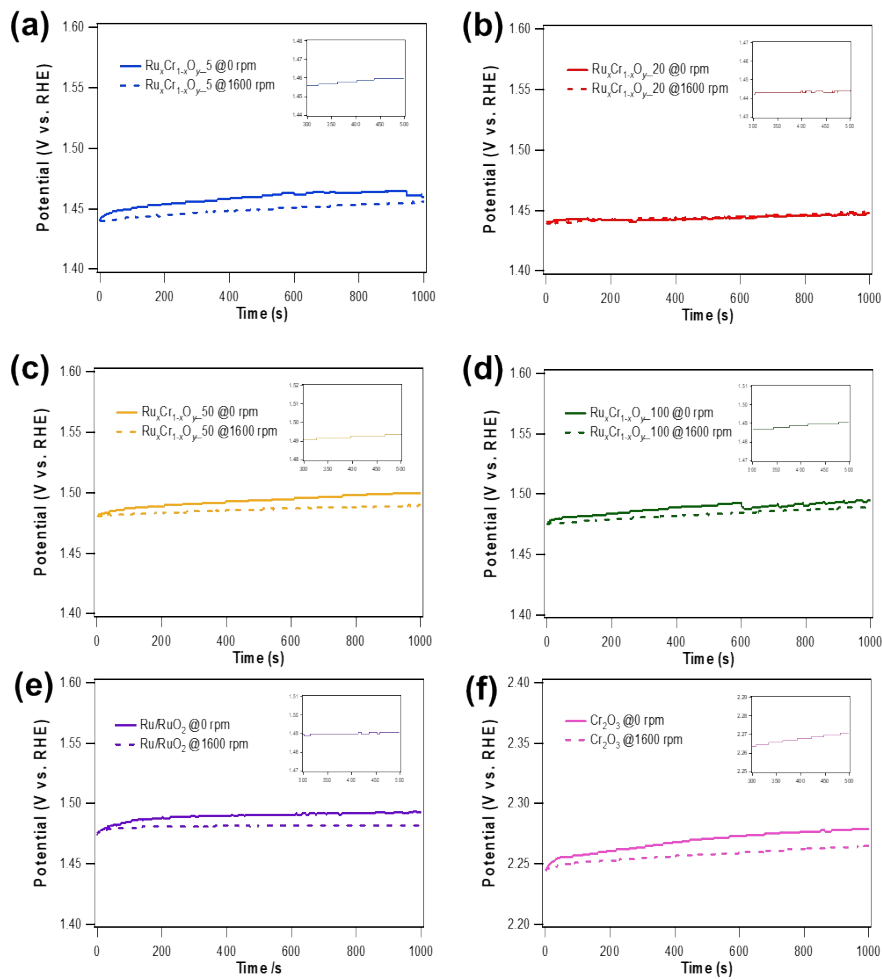


Fig. S19. Chronopotentiometric monitoring of generated O_2 gas desorption for (a) $Ru_xCr_{1-x}O_y-5$, (b) $Ru_xCr_{1-x}O_y-20$, (c) $Ru_xCr_{1-x}O_y-50$, (d) $Ru_xCr_{1-x}O_y-100$, (e) Ru/RuO₂ and (f) Cr₂O₃ in 0.5 M H_2SO_4 aqueous solution. Constant current of 5 mA cm^{-2} was applied for 1000-s continuous OER (Insets: potential changes measured between 300 and 500 s).